Unsupervised Multiresolution Segmentation for Images with Low Depth of Field

James Z. Wang, *Member*, *IEEE*,
Jia Li, *Member*, *IEEE*,
Robert M. Gray, *Fellow*, *IEEE*, and
Gio Wiederhold, *Fellow*, *IEEE*

Abstract—Unsupervised segmentation of images with low depth of field (DOF) is highly useful in various applications including image enhancement for digital cameras, target recognition, image indexing for content-based retrieval, and 3D microscopic image analysis. This paper describes a novel multiresolution image segmentation algorithm for low DOF images. The algorithm is designed to separate a sharply focused object-of-interest from other foreground or background objects. The algorithm is fully automatic in that all parameters are image independent. A multiscale approach based on high frequency wavelet coefficients and their statistics is used to perform context-dependent classification of individual blocks of the image. Unlike other edge-based approaches, our algorithm does not rely on the process of connecting object boundaries. The algorithm has achieved high accuracy when tested on more than 100 low DOF images, many with inhomogeneous foreground or background distractions. Compared with the state of the art algorithms, this new algorithm provides better accuracy at higher speed.

Index Terms—Content-based image retrieval, image region segmentation, low depth-of-field, wavelet, multiresolution image analysis.

1 Introduction

UNSUPERVISED image segmentation [7] is invariably one of the most challenging problems in computer vision. In this paper, we focus on the segmentation of low depth of field (DOF) images. Segmentation of images with low DOF is also crucially important in applications such as image enhancement for digital cameras, target recognition [2], image indexing for content-based retrieval [6], [8], [20], [21], [12], and 3D microscopic image analysis. Low DOF is an important technique widely used by professional photographers for various types of images, such as telephoto images, to emphasize a certain object. It is also a key technique for microbiologists to understand the 3D structure within a specimen under a high-power microscope.

Normal human vision is nearly infallible in segmenting sharply focused objects-of-interest in a low DOF image. Often, both global and local image characteristics are utilized by the human visual system while segmenting images. We have developed a fully automatic multiresolution segmentation algorithm for low DOF images. The algorithm is designed to separate sharply focused objects-of-interest from other foreground or background objects.

The outline of this paper is as follows: In Section 2, we introduce the low depth of field and its relationship with image segmentation. In Section 3, image features used in our segmentation algorithm are described. The details of the segmentation algorithm are provided in Section 4. In Section 5, experimental results on real-world image data are presented. Finally, we draw conclusions and point out future directions in Section 6.

- *J.Z. Wang is with the School of Information Sciences and Technology, Pennsylvania State University, 120 S. Burrowes Street, University Park, PA 16801. E-mail: wangz@cs.stanford.edu.*
- *J. Li is with the Department of Statistics, Pennsylvania State University, 326 Thomas Building, University Park, PA 16802. E-mail: jiali@stat.psu.edu.*
- *R.M. Gray is with the Department of Electrical Engineering, Stanford University, Stanford, CA 94305. E-mail: rmgray@stanford.edu.*
- *G. Wiederhold is with the Department of Computer Science, Stanford University, Stanford, CA 94305. E-mail: gio@cs.stanford.edu.*

Manuscript received 2 Feb. 1999; revised 23 Feb. 2000; accepted 3 Aug. 2000. Recommended for acceptance by C.A. Bouman.
For information on obtaining reprints of this article, please send e-mail to: tpami@computer.org, and reference IEEECS Log Number 109114.

2 Background

In this section, we briefly describe the concept of depth of field in photography and its relationship with image segmentation. Low DOF is an important photographic technique commonly used to assist readers in understanding the depth information within a 2D photograph (Fig. 1). Low DOF is also common in microscopic images.

For convenience, we call the sharply focused object-of-interest the **OOI** and the out-of-focused foreground and background objects the **background**. In actuality, some background objects may be closer to the camera than the OOI (Fig. 1).

2.1 Depth of Field

Depth of field (DOF) is the range of distance from a camera that is acceptably sharp in the photograph [1], [17]. A typical camera is an optical system containing a lens and an image screen. The lens creates images in the plane of the image screen which is normally parallel to the lens plane. Note that the lens plane may not always be parallel to the plane of image screen. For example, control of perspective and depth-of-field can be achieved using tilt-and-shift movements of the lens or the film plane in a large format view camera [1]. Fig. 2 illustrates the optical construction of a typical camera.

Denote the focal length of the lens by f and its diameter by a. Denote the aperture f-stop number for this photo by p. Then, $f = ap$. Suppose the image screen is at distance d from the lens and the object is at distance s from the lens. If the object is in focus, then the Gaussian thin lens law holds: $\frac{1}{s} + \frac{1}{d} = \frac{1}{f}$.

A point closer or farther away from the lens than s is imaged as a circle, as shown in Fig. 2. Assume the largest circle that a human can tolerate, namely, the circle of minimum confusion, has a diameter of c. A point is considered sharp if and only if the image of the point is smaller than the circle of minimum confusion. As shown in Fig. 2, d_f and d_r are the front and the rear DOF limits, respectively.

By simple geometry, it can be shown that

$$d_f = \frac{scp(s-f)}{f^2 + cp(s-f)},\ d_r = \frac{scp(s-f)}{f^2 - cp(s-f)}.$$

Usually the size of the circle of minimum confusion is fixed for a given image size. For a fixed circle of minimum confusion, we conclude from the above equations that larger aperture, closer object distance, or longer focal length, leads to lower DOF (e.g., Fig. 3).

2.2 Low DOF and Photography

With low DOF, only the OOI is in sharp focus, whereas background objects are typically blurred to out-of-focus. Photographers often use low DOF to create a sense of depth in two dimensional photographs. Examples are shown in Fig. 3. For example, in a typical sports image such as Fig. 3a, the player is much sharper than the background crowds. We know immediately that the player is in the foreground and is the OOI. Images obtained from microscopes are usually of low DOF (Fig. 3e).

2.3 Low DOF and Image Segmentation

The normal human vision system (HVS) is nearly infallible in depth perception of both low DOF and high DOF photographs. For the case of understanding high DOF photographs, human knowledge plays a key role. For example, the HVS is capable

Fig. 1. Human knowledge is critical in depth perception for images with high DOF. (a) An image with high DOF. (b) An image with high DOF.

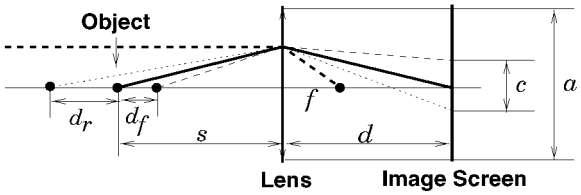

Fig. 2. The optical construction of a typical camera.

of interpreting a lake in a scene as a flat surface. The HVS can also understand cartoon sketches when no detailed texture information is available.

On the other hand, for images with substantially distinct depths, such as images with low DOF, the sharpness of objects assists our depth perception. Low DOF is often preferred by professional photographers when taking a photograph with distracting background objects. Low DOF microscopic imaging is also important for microbiologists who use a low DOF microscope to determine the 3D structure of a specimen from 2D slices.

2.4 Related Work

Recent work has taken advantages of DOF in the field of computer vision and image understanding [4], [11], [14], [18], [15], [22]. Yim and Bovik [22] have explored the possibility of depth perception using a sequence of images taken with different image plane distances. Yim and Bovik [22] have also provided a detailed survey of these techniques.

Tsai and Wang [19] recently proposed an edge-based segmentation algorithm for similar applications. The amount of defocus at each edge pixel is evaluated using the moment-preserving principle. The algorithm has demonstrated high accuracy for segmenting man-made objects and objects with clear boundary edges. However, the algorithm is not suitable for segmenting natural objects (e.g., Fig. 4a) with blunt edges because of the dependence of an edge-linking procedure to find the closed boundaries in the algorithm.

Normal region segmentation algorithms, including the edge flow algorithm [13], the normalized cut algorithm [16], and the Gaussian mixture model algorithm [3], are also not suited to this problem. These algorithms decompose an image into regions each containing relatively uniform color and texture without indication of whether a region is part of the OOI or background. Fig. 4b shows the segmentation results using the image segmentation algorithm reported in [3].

Our algorithm detects the sharply focused objects in a low DOF image by using multiresolution wavelet frequency analysis and statistical methods. In fact, sharply focused objects have more details within the object than the out-of-focus background. As a result, the focused object regions have more high-value wavelet coefficients in the high frequency bands of the transform. In our algorithm, we do not rely on the distinction in color between the object and the background, or the existence of closed boundaries of the objects. By analyzing the details of the regions rather than analyzing the colors or the boundary edges, our algorithm is potentially more robust than region-based or edge-based segmentation algorithms when processing natural scenes.

3 Segmentation Features

We partition an image into blocks and classify each block as *background* or *object-of-interest*. The classifier uses two features, the average intensity of an image block and the variance of wavelet coefficients in the high frequency bands. The average intensity is used to test how similar one block is to another. The variance of wavelet coefficients in the high frequency bands is the main feature to distinguish background and OOI.

Because only the OOI is in focus in a low DOF image, details in the OOI are captured but those in background are not. The details in the OOI result in larger high frequency energy in an image. We measure the high frequency energy by the variance of wavelet coefficients in the high frequency bands, i.e., the LH, HL, and HH bands shown in Fig. 5. For any image block, the variance of wavelet coefficients at the same spatial location in the three high frequency bands is used as a feature for the image block. We denote this feature as v.

Suppose an image is specified by a set of pixels $\mathcal{I} = \{(m,n),\ m = 0,\ldots,M-1,\ n = 0,\ldots,N-1\}$ and its wavelet coefficients are $\{w_{m,n},\ (m,n) \in \mathcal{I}\}$. Without loss of generality, consider block $\{(m,n),\ m = 0,\ldots,s-1,\ n = 0,\ldots,s-1\}$. The wavelet coefficients for the block in LH, HL, and HH bands are

$$\{w_{m,n}, m = 0,\ldots,s/2-1,\ n = N/2,...,N/2+s/2-1\},$$

$$\{w_{m,n}, m = M/2,\ldots,M/2+s/2-1,\ n = 0,\ldots,s/2-1\},$$

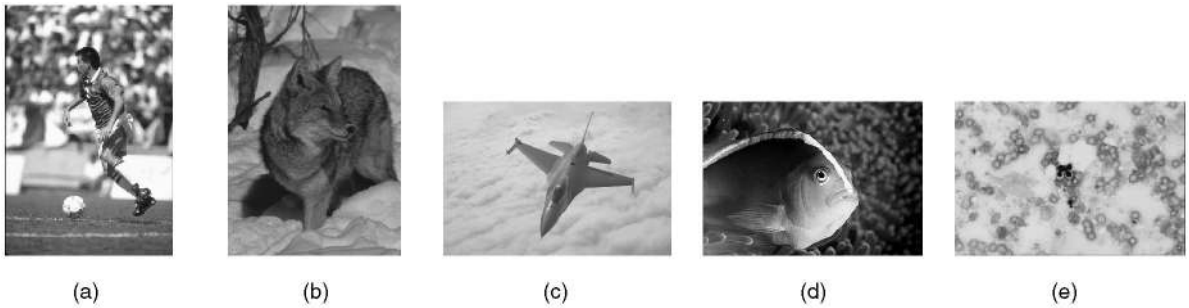

Fig. 3. Types of images with low DOF. (a) Sport—long focal length, (b) telephoto—long focal length, (c) close-up—large aperture, (d) macro—close distance, and (e) microscopic—close distance.

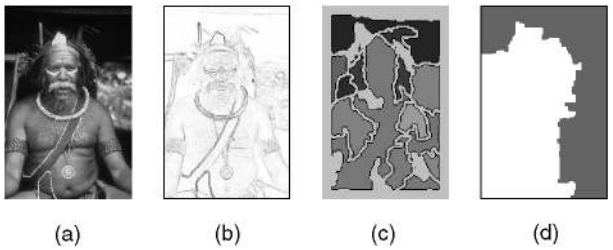

Fig. 4. Segmentation of a low DOF image. (a) Original image. (b) OOI may not have sharp boundary edges. (c) Traditional region-based segmentation is not suitable. (d) Our low DOF segmentation.

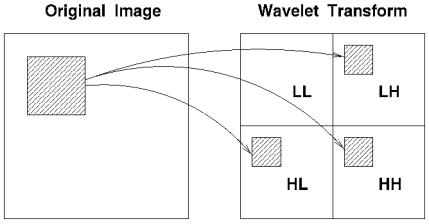

Fig. 5. The wavelet coefficients at the same spatial location in the high frequency bands for a block in an image.

and

$$\{w_{m,n}, m = M/2, \ldots, M/2 + s/2 - 1, \\ n = N/2, \ldots, N/2 + s/2 - 1\},$$

respectively. The feature v is then calculated as the variance of the wavelet coefficients in all the three sets. For other shifted image blocks, their wavelet coefficient blocks for calculating v are shifted correspondingly, as shown in Fig. 5.

In our current implementation, the Haar wavelet transform [5] is used because of its good localization property provided by its short filter. We expect other Daubechies' wavelet transforms [5] with short length filters to give similar results. The Haar transform is selected in particular since the computational cost is the lowest among all the wavelet transforms. Fig. 6 shows a comparison among the Canny edge detection, the Tsai algorithm [19], and a wavelet transform. The OOI stands out more distinctly in the high frequency band of the wavelet transform than that does in the traditional edge detected image.

4 The Algorithm

The classification algorithm consists of three steps:

1. initial classification at the lowest scale,
2. a recursive process to adjust the crude classification result using a multiscale approach, and
3. postprocessing to obtain smooth boundaries and to remove small isolated regions.

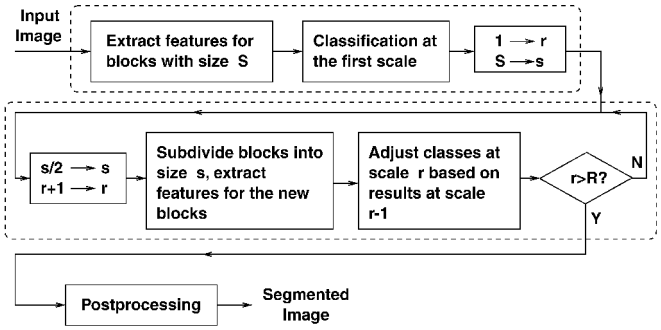

Fig. 7. The main components of the algorithm.

As shown in Fig. 7, we start with a large block size. A crude classification is performed with the large blocks. At every increased scale, the blocks are subdivided into four *child* blocks, forming a quad-tree structure. Child blocks inherit the classes of parent blocks as their initial classes. The classifier then adjusts the classes of the child blocks according to their features and their context, which is represented by the statistics of their neighboring blocks. After the adjustment is performed, the classifier increases the scale and repeats the previous step until the maximum scale is reached. This multiscale approach is motivated by a similar context-dependent classification structure, developed, and applied to document segmentation by Li and Gray [10].

4.1 Initial Classification

For the initial classification, we start with a large block size $S \times S$, which is usually set to 32×32 for an image of around 768×512 pixels in our applications. We denote the lowest scale by $r = 0$. By avoiding overlocalization, large blocks provide a more discerning feature v, defined in the previous section, for the two classes: background and OOI. Since classification performed on the large blocks is crude, we compensate this by adjusting the classes at higher scales.

Denote the blocks at scale $r = 0$ by $\mathcal{S}^{(0)} = \{(i,j), i = 0, \ldots, I,\ j = 0, \ldots, J\}$ and the feature v for the blocks by $v_{i,j}, (i,j) \in \mathcal{S}^{(0)}$. We then partition $v_{i,j}$ into two clusters using the k-means clustering algorithm [9]. One cluster represents the background and the other represents the OOI. In the view that the OOI has a higher average v, we set the cluster with the higher average v as the OOI class. Denote the background cluster center by $v^{(0)}$, and the OOI cluster center by $v^{(1)}$. The k-means algorithm determines the class of block (i,j), $(i,j) \in \mathcal{S}^{(0)}$, at scale $r = 0$, by $c_{i,j} = \min_{k=0,1}^{-1}(v_{i,j} - v^{(k)})^2$.

At the end of the initial classification, we delete small isolated background regions to avoid smooth regions of the OOI being classified incorrectly.

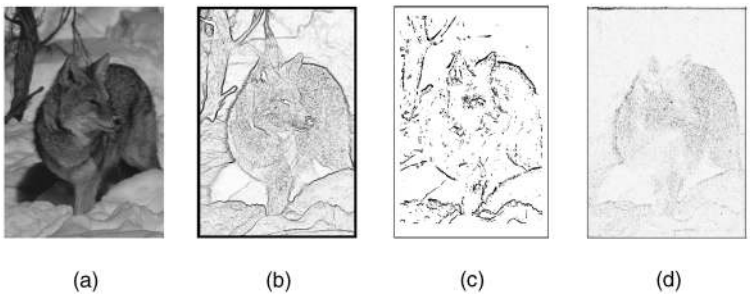

Fig. 6. Comparison of the traditional edge detection and wavelet transform. (a)Original image. (b) Canny edge detection. (c) Tsai edge detection. (d) High frequency band of WT.

Fig. 8. The sequence of multiscale refinement results.

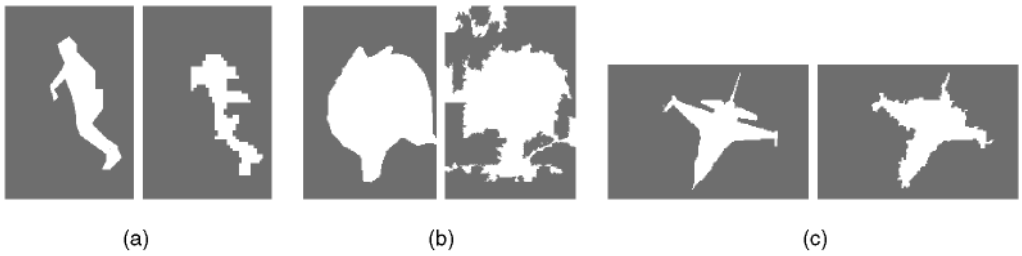

Fig. 9. The computer segmentation (right) is close to the human segmentation (left). (a) Sport, (b) fox, and (c) jet plane.

4.2 Multiscale Context Dependent Classification

The second step in the classification is to adjust the segmentation result obtained in the first step using context information through a multiscale approach. At each increased scale, the blocks are partitioned into a quad-tree with four child blocks. The parent block of block (i,j) is denoted by $(\tilde{i},\tilde{j})$, where $\tilde{i}=\lfloor i/2\rfloor$, $\tilde{j}=\lfloor j/2\rfloor$. Denote the set of blocks at scale r by $\mathcal{S}^{(r)}$, $r=1,\ldots,R$, where R is the maximum scale set by users. The block size at scale R is the finest resolution that a user needs. We choose R as the scale at which one block is a single pixel in our applications.

The feature v and the average intensities of blocks at scale r are evaluated. The initial classes of the blocks are set to the classes of their parent blocks. For every block which is adjacent to a block with a different class, the classifier decides whether to switch the class of one of the blocks according to their v, and the similarity to their parent blocks.

The multiscale approach is used to solve the conflict of overlocalization and high resolution classification. By gradually reducing the block size, the classifier can track the more global properties of a block through its parent block. At the same time, a high resolution classification is achieved eventually. The details of the algorithm are provided in the list below:

1. Set $1\rightarrow r$.
2. Partition blocks in $\mathcal{S}^{(r)}$ into blocks in $\mathcal{S}^{(r+1)}$. Set $r+1\rightarrow r$.
3. Calculate features $v_{i,j}$ and average intensities $x_{i,j}$ for blocks $(i,j)\in\mathcal{S}^{(r)}$.
4. For each block $(i,j)\in\mathcal{S}^{(r)}$ at the boundary of the OOI, i.e., the block itself belongs to the OOI and at least one of its four neighbors is segmented as background, adjust the classes as follows:
   a. Set $0\rightarrow k$.
   b. For the kth neighbor block (m,n), set $flip_{background}=1$ if one of the following conditions is satisfied:
      i. The difference between the average intensity $x_{m,n}$ of block (m,n) and that of its parent block is larger than both a threshold and the difference between $x_{m,n}$ and the average intensity of the parent block of (i,j).
      ii. The feature $v_{i,j}$ is closer to the center of the OOI cluster, i.e., $(v_{i,j}-v^{(1)})^2<(v_{i,j}-v^{(0)})^2$.
   c. For the kth neighbor block (m,n), set $flip_{OOI}=1$ if one of the following conditions is satisfied:
      i. The difference between the average intensity $x_{i,j}$ of block (i,j) and that of its parent block is larger than the difference between $x_{i,j}$ and the average intensity of the parent block of (m,n), and $|x_{i,j}-x_{\tilde{m},\tilde{n}}|<\theta$, where θ is a threshold.
      ii. The difference between the average intensity $x_{i,j}$ of block (i,j) and that of its parent block is larger than the difference between $x_{i,j}$ and the average intensity of the parent block of (m,n), and $v_{i,j}$ is much closer to $v^{(0)}$.
   d. If $flip_{OOI}=1$ and $flip_{background}=0$, switch the class of block (i,j) to background.
   e. If $flip_{OOI}=0$ and $flip_{background}=1$, switch the class of block (m,n) to the OOI.
   f. If block (i,j) is switched to background, for any of its neighboring blocks that has been switched from background to OOI, change the class of this block back to background.
   g. If $k=3$, go to Step 5; else, $k+1\rightarrow k$, go to Step 4b.
5. If $r\leq R$, go to Step 2; else, stop.

The algorithm above checks all the OOI blocks adjacent to background blocks and switches the classes of the block and its neighbors if needed. Since all background blocks adjacent to an OOI block are compared to the OOI block, it is thus redundant to go through all the background blocks as well and compare them with their neighboring blocks. The thresholds used in the algorithm are preselected and fixed for any test image. Note that the cluster centers $v^{(0)}$ and $v^{(1)}$ for background and OOI are fixed through all the scales. Also, the features $v_{i,j}$ are discarded at very high scales. When the scale is sufficiently high, the blocks shrink to very small sizes. Small blocks in both background and OOI are likely to be smooth, thus $v_{i,j}$, which are the variances of wavelet coefficients in the high frequency bands, are no longer good indicators for classes. Thus, we use the segmentation results obtained from previous scales as context and classify based only on the closeness of average intensities.

TABLE 1
The Segmentation Results of Our Algorithm

Image	Resolution	Sen.	Spec.	P_e
(a)	256×172	73.7%	97.5%	5.5%
(b)	768×512	90.7%	80.1%	16.1%
(c)	512×768	97.5%	96.4%	3.4%

Fig. 10. The segmentation results of our algorithm.

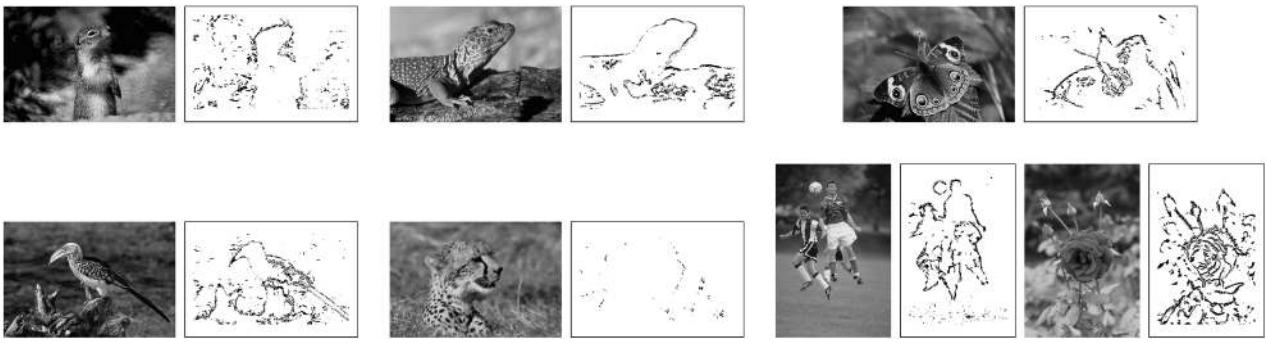

Fig. 11. The segmentation results of the algorithm developed by Tsai and Wang [19].

The algorithm examines blocks on the boundaries of OOI and background because the boundary regions are most likely to be classified incorrectly. Consequently, the algorithm can be viewed as a multiscale edge refiner. At the boundary regions, a parent block may contain both classes. A subblock which is incorrectly segmented as the class of its parent block is likely to have properties rather different from its parent block. In our case, the properties are the feature v and the average intensity. If a subblock happens to have a closer average intensity to those of its neighboring blocks with the other class and its own feature v is also closer to the other class, we switch its class.

After the multiscale refining of edges is completed, the segmented image is passed through a postprocessor which removes small isolated regions and smoothes the boundaries.

5 Experimental Results

The system has been implemented by C on UNIX platforms. The experiments were performed on a single-CPU 300 MHz Pentium PC with the Linux operating system. The algorithm has achieved high accuracy when tested on more than 100 low DOF images downloaded from the World Wide Web or selected from the JPEG-compressed COREL CD-ROM image collection. In general, the total error rate is less than 10 percent. Most of the test images have inhomogeneous foreground or background distractions. The segmentation results obtained were very close to the human partitioning of these images. Besides its high accuracy, the algorithm is very fast. An image of 768×512 pixels can be segmented within two seconds.

An example is shown in Fig. 8 to illustrate how the progressive segmentation proceeds. Six scales are used starting with block size 32×32 and going to 1×1. Fig. 9 shows the segmentation results for images in Figs. 3a, 3b, and 3c. We evaluate classification performance by *sensitivity*, *specificity*, and error rate. Sensitivity is defined as the ratio of the area of the OOI identified to the total area of OOI in the image. Specificity is defined as the ratio of the area of the background identified to the total area of the background in the image.

For segmented images shown in Fig. 9, the sensitivity, specificity, and error rate (P_e) are provided by Table 1. For a typical low DOF image, such as the jet plane image, the sensitivity and specificity are both above 95 percent. For a more difficult image, such as the fox image, the system demonstrates a high accuracy of 90 percent sensitivity and 80 percent specificity. The rear legs of the fox are not segmented correctly because they are not fully focused. The performance on the sport image is lower because the image is of low resolution and low quality. In general, the system performs well when the resolution is higher than 200×200 and when the JPEG compression ratio is lower than $5:1$. The ball is not included in the human segmentation because it is not fully focused. More segmentation results are provided in Fig. 10. We compared our results with the edge-based algorithm in [19]. As shown in Fig. 11, the edge-based algorithm failed to detect the edges of the OOI.[1]

Our algorithm has the following limitations:

1. It is not designed to segment those low DOF images for which some high-level human knowledge or image stereo is required in the region determination process. Unlike many other edge-based segmentation algorithms, we rely on the sharp details of the OOI. However, if the OOI is highly smooth, the algorithm may fail.
2. It is designed to segment sharply focused OOI. For some applications, the DOF may be so low that the OOI itself include out-of-focus regions. The algorithm is not capable of segmenting the entire OOI in this case, e.g., the fox image.
3. The performance of the algorithm is lower when the image resolution or the image quality is low, e.g., the sport image.

1. Edge-detection results were provided by the authors of [19]. We were informed that their edge-linking process and final segmentation were unsuccessful.

6 Conclusions and Future Work

In this paper, we have demonstrated a novel unsupervised multiresolution image segmentation algorithm for low DOF images. A multiscale approach based on high frequency wavelet coefficients and their statistics is used to perform context-dependent classification of individual blocks. Segmenting images with high DOF or images requiring human knowledge will still be highly challenging. However, the accuracy of this algorithm may be improved for images with low DOF by designing a better feature and using a better statistical clustering algorithm. It is also useful to design an algorithm that is capable of classifying an image as a low DOF image or a high DOF image. The algorithm can be used in indexing image databases for content-based retrieval. At last, the algorithm can be extended to problems such as biomedical image segmentation.

Acknowledgments

This work was supported in part by the US National Science Foundation under grant MIP-9706284 and grant IIS-9817511. The authors would like to thank Oscar Firschein, visiting scholar at Stanford University, and various researchers including Martin A. Fischler and Quang-Tuan Luong of the SRI AI Center for the valuable discussions in computer vision and photography. They would like to thank Du-Ming Tsai for providing comparison results. They would also like to thank the reviews for their constructive comments. Research was performed when J.Z. Wang was with the Departments of Computer Science and Medical Informatics, Stanford University and J. Li was with the Department of Electrical Engineering, Stanford University.

References

[1] A. Adams, *The Camera.* Boston: New York Graphic Soc., 1980.
[2] Y. Boykov and D. Huttenlocher, "A New Baysian Framework for Object Recognition," *Proc. DARPA IU Workshop*, 1998.
[3] C. Carson, S. Belongie, H. Greenspan, and J. Malik, "Blobworld: Image Segmentation Using Expectation-Maximization and Its Application to Image Querying," submitted for publication.
[4] T. Darell and K. Wohn, "Depth from Focus Using a Pyramid Architecture," *Pattern Recognition Letters,* vol. 11, no. 12, pp. 787-96, Dec. 1990.
[5] I. Daubechies, *Ten Lectures on Wavelets.* Philadelphia: SIAM, 1992.
[6] C. Faloutsos, R. Barber, M. Flickner, J. Hafner, W. Niblack, D. Petkovic, and W. Equitz, "Efficient and Effective Querying by Image Content," *J. Intelligent Information Systems,* vol. 3, pp. 231-262, 1994.
[7] R.G. Gonzalez and R.E. Woods, *Digital Image Processing.* Reading, Mass.: Addison-Wesley, 1992.
[8] A. Gupta and R. Jain, "Visual Information Retrieval," *Comm. ACM,* vol. 40, pp. 69-79, 1997.
[9] A. K. Jain, R. C. Dubes, *Algorithms for Clustering Data.* Englewood Cliffs, N.J.: Prentice-Hall, 1988.
[10] J. Li and R.M. Gray, "Context-Based Multiscale Classification of Images," *Proc. IEEE Int'l Conf. Image Processing,* Oct. 1998
[11] E. Krotkov, *Active Computer Vision by Cooperative Focus and Stereo.* New York: Springer-Verlag, 1989.
[12] J. Li, J.Z. Wang, and G. Wiederhold, "IRM: Integrated Region Matching for ImageRetrieval," *Proc. 2000 ACM Multimedia Conf.,* Oct. 2000.
[13] W.Y. Ma and B.S. Manjunath, "Edge Flow: A Framework of Boundary Detection and Image Segmentation," *Proc. Computer Vision and Pattern Recognition,* pp. 744-749, 1997.
[14] S.K. Nayar and Y. Nakagawa, "Shape from Focus," *IEEE Trans. Pattern Analysis and Machine Intelligence,* vol. 16, no. 8, pp. 824-831, Aug. 1994.
[15] M. Noguchi and S.K. Nayar, "Microscopic Shape from Focus Using a Projected Illumination Pattern," *Math. and Computer Modelling,* vol. 24, nos. 5/6, pp. 31-48, Sept. 1996.
[16] J. Shi and J. Malik, "Normalized Cuts and Image Segmentation," *Proc. Computer Vision and Pattern Recognition,* pp. 731-737, 1997.
[17] *Basic Photographic Materials and Processes,* L. Stroebel, ed. Boston: Focal Press, 1990.
[18] M. Subbarao, T. Yuan, and J.-K. Tyan, "Integration of Defocus and Focus Analysis with Stereo for 3D Shape Recovery," *Three-Dimensional Imaging and Laser-Based Systems for Metrology and Inspection III,* pp. 14-15, Oct. 1997.
[19] D.-M. Tsai and H.-J. Wang, "Segmenting Focused Objects in Complex Visual Images," *Pattern Recognition Letters,* vol. 19, no. 10, pp. 929-940, Aug. 1998.
[20] J.Z. Wang, G. Wiederhold, O. Firschein, and X.W. Sha, "Content-Based Image Indexing and Searching Using Daubechies' Wavelets," *Int'l J. Digital Libraries,* vol. 1, no. 4, pp. 311-328, 1998.
[21] J.Z. Wang, J. Li, D. Chan, and G. Wiederhold, "Semantics-Sensitive Retrieval for Digital Picture Libraries," *D-LIB Magazine,* vol. 5, no. 11, Nov. 1999. http://www.dlib.org.
[22] C. Yim and A.C. Bovik, "Multiresolution 3D Range Segmentation Using Focus Cues," *IEEE Trans. Image Processing,* vol. 7, no. 9, pp. 1283-1299, 1998.